New Journal of Physics
The open access journal at the forefront of physics
Deutsche Physikalische Gesellschaft DPG | IOP Institute of Physics

Magnetic exchange force microscopy from first principles: application to the antiferromagnetic NiO(001) surface

Mihail Granovskij[1,2,3], **Andreas Schrön**[1,2] **and Friedhelm Bechstedt**[1,2]

[1] Institut für Festkörpertheorie und -optik, Friedrich-Schiller-Universität, Max-Wien-Platz 1, D-07743 Jena, Germany
[2] European Theoretical Spectroscopy Facility (ETSF)
E-mail: mihail.granovskij@gmail.com

Received 4 November 2013, revised 12 December 2013
Accepted for publication 16 December 2013
Published 7 February 2014

New Journal of Physics **16** (2014) 023020

doi:10.1088/1367-2630/16/2/023020

Abstract

We present an accurate *ab initio* description of the magnetic exchange force microscopy (MExFM). As a prototypical system, the antiferromagnetic NiO(001) surface probed with a Fe tip is investigated. The tip–surface interaction is described on two levels. Short-range chemical and exchange forces between the tip apex and the surface atoms are described in the framework of spin-polarized density functional theory while long-range van der Waals forces are considered within a mesoscopic tip model. For the Ni atoms in the NiO surface as well as the Fe atoms of the tip apex, an on-site repulsion U in the transition-metal 3d shells is included. In order to understand the tip–surface interaction, we investigate the changes in the electronic structure of tip and surface versus distance. The resulting frequency shifts and MExFM images are in good qualitative agreement with experimental data.

1. Introduction

Besides the interest in fundamentals of magnetic phenomena, developments toward high-resolution magnetic imaging are driven by demands of modern magnetic data storage and

[3] Author to whom any correspondence should be addressed.

logical devices at atomic scale [1, 2]. In this development surface-sensitive techniques play an important role. The direct visualization of spin structures with atomic-scale resolution is, however, a challenge for both experiment and theory.

Combining the atomic resolution of scanning tunneling microscopy (STM) with spin sensitivity, spin-polarized (SP)-STM provides unprecedented insight into collinear and non-collinear spin structures at surfaces of conducting magnetic solids and their nanostructures [3–6]. However, (SP-)STM techniques cannot be applied directly to surfaces of insulators. In order to achieve conductivity of the sample it has to be either doped [7, 8] or locally irradiated with an electron beam [9]. Direct access to atomic resolution on insulating surfaces is provided by non-contact atomic force microscopy (NC-AFM) by sensing the short-range chemical interaction between tip atoms and surface atoms underneath [6, 10]. Spin imaging is achieved by detecting the short-range magnetic interaction such as the exchange interaction between a ferromagnetic tip and a magnetic sample and is, hence, called magnetic exchange force microscopy (MExFM) [6, 11–13]. Its performance has been clearly demonstrated for the (001) surface of antiferromagnetic NiO [13, 14] as well as an antiferromagnetically ordered Fe monolayer on W(001) [15].

The 3d transition-metal monoxides (TMOs) attract much attention in condensed matter physics because of their promising electronic and magnetic properties for information technology and spintronics. This holds especially for their surfaces and nanostructures [16]. At high temperatures, the 3d TMOs crystallize in an ideal rocksalt structure and show paramagnetic behavior. Below their respective Néel temperature, the magnetic moments of the TM^{2+} ions arrange in the antiferromagnetic ordering AFM II, and a small perturbation of the ideal rocksalt structure occurs [17]. Superexchange mediated by the O^{2-} ions has been identified to be the driving mechanism behind the formation of the antiferromagnetic ordering [18, 19]. The insulator NiO serves as a prototypical sample system: (i) due to its high Néel temperature of 525 K [20], NiO exhibits the antiferromagnetic ordering at room temperature. (ii) The cleavage (001) surface is stable and displays the antiferromagnetic ordering of the bulk. It is therefore easily accessible for experimental surface probe measurements [6, 13].

Ab initio calculations by means of spin-polarized density functional theory (DFT) [21, 22] have contributed to an understanding of the atomic geometry, the electronic structure and the magnetic interactions of the NiO(001)2×1 surface [23–25]. However, the results depend on the description of exchange and correlation (XC), in particular, the local electron interaction on the Ni 3d shell, e.g. described by an on-site Coulomb U parameter [26]. Apart from the details of the geometry and electronic states of the NiO(001)2×1 surface, there remain open questions. This is true for the theoretical description of atomic-scale scanning probe techniques such as NC-AFM and MExFM. The central question concerns the tip–sample interaction, the variation of chemical forces and magnetic exchange forces versus distance and their relative contribution to the total forces. While the influence of the chemical nature of the tip material has been studied theoretically and experimentally [27, 28], the mutual interaction, in particular the redistribution of electron and magnetization densities in the tip apex and the surface due to their interaction are less understood. Another difficulty of understanding concerns the magnetic contrast which unambiguously reveals the antiferromagnetic ordering of NiO(001). It could not be observed experimentally until recently [13, 27]. In addition to that, it was shown that even with the same experimental setup, the magnetic contrast depends on the chosen frequency shift or, equivalently, the minimum tip–surface distance [13]. The determination of optimum

conditions to achieve a large magnetic signal is one of the important issues for experimental setups.

First theoretical attempts to understand the tip–surface interaction have been made by applying the unrestricted Hartree–Fock (UHF) method [29] or DFT within the local spin density approximation (LDA) [30]. However, neither of these methods describe the Coulomb interaction of the TM 3d electrons properly [31, 32]. In particular, the on-site Coulomb repulsion is either strongly overestimated (UHF) or underestimated (LDA) [31, 32]. Further limitations of these early attempts were due to the available computer resources. The tip apex was described by only one individual atom. Moreover, these studies were restricted to a few self-consistent calculations at several heights and, hence, a fitting of the potential energy [29] or force curves [30] to model functions was inevitable. Such an approach, however, can only give a rough description of the tip–surface interaction and its dependence on the tip–surface separation.

In the present paper, we study the tip–surface interaction for the prototypical sample, the antiferromagnetic NiO(001) surface probed with a ferromagnetic Fe tip, within the framework of spin-polarized DFT. The electronic interaction of the TM 3d shell is properly described with an on-site Coulomb parameter U. Besides the short-range chemical and magnetic forces obtained within the LDA+U approach also long-range van der Waals (vdW) forces are considered. A dense sampling of the tip–surface distance allows a study of the details of chemical and magnetic forces. The resulting MExFM images are discussed and a physical explanation, particularly for the spin contrast, is given. In section 2, the theoretical model used to calculate MExFM images and the treatment of the different long- and short-range forces are described. The short-range tip–surface interaction is investigated in detail in section 3. Finally, the resulting MExFM images and corrugations are presented in section 4. A brief summary and conclusions follow in section 5.

2. Theoretical modeling

2.1. Frequency shifts and forces

We follow the description of a NC-AFM given in [33]. The cantilever with spring constant k oscillates with the amplitude A at the resonance frequency $f = f_0 + \Delta f$ which is shifted by Δf from the resonance frequency of the unperturbed cantilever f_0 due to the forces between tip and sample. In the constant-force mode of operation, the average force acting on the tip over one cycle and, hence, the frequency shift Δf are kept constant. In general, the frequency shift Δf depends strongly on the various parameters of the experimental setup [33]. However, if the amplitude A is much larger than the range of the forces acting between tip and sample, a normalized frequency shift $\gamma = kA^{3/2}\Delta f/f_0$ that is independent of any experimental parameters can be introduced [34]. For typical oscillation amplitudes [13] of more than 50 Å, this large-amplitude approximation is a good approximation. Within the large-amplitude approximation, the normalized frequency shift is given as [33]

$$\gamma(d; x, y) = \frac{1}{\sqrt{2}\pi} \int_d^\infty \frac{F_{\mathrm{ts}}(x, y, z)}{\sqrt{z-d}} dz, \tag{1}$$

where $F_{\mathrm{ts}}(x, y, z)$ is the force between tip and surface, if the tip is located at the height z over the surface at the lateral position (x, y). d is the minimum tip–surface distance during one oscillation cycle. Different contributions to the tip–surface interaction F_{ts}, such as long-range vdW forces, short-range chemical and exchange-correlation forces, but also electrostatic

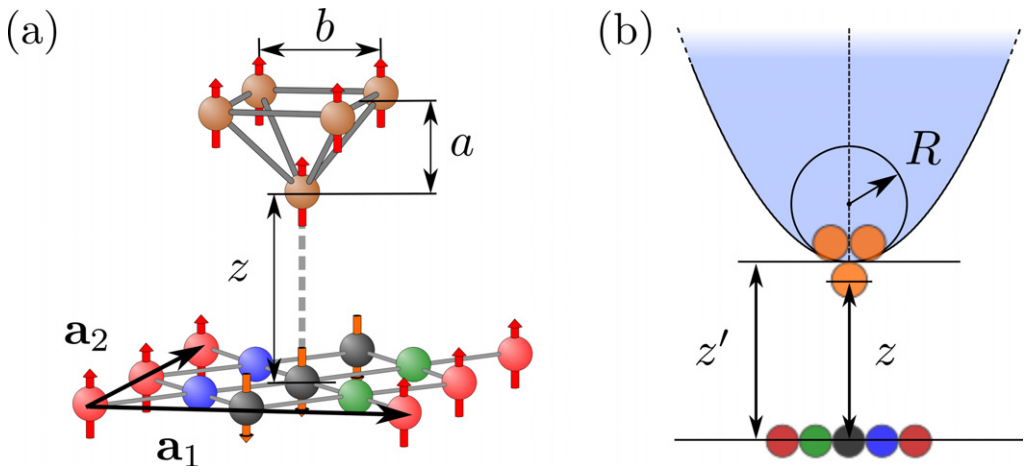

Figure 1. (a) $p(2\times 2)$ unit cell of the NiO(001) surface with the microscopic pyramidal tip apex. Red (black) spheres indicate Ni^{2+} ions. Blue (green) spheres represent O^{2-} ions with underlying spin-up (spin-down) Ni^{2+} ions in the first sub-surface layer. Brown spheres display the Fe atoms in the tip. The arrows indicate the orientation of the magnetization of the various atoms. (b) Long-range vdW forces are considered for a mesoscopic parabolic tip. The apex of the mesoscopic tip z' is assumed to intersect the microscopic pyramidal tip at half of the microscopic tip height, such that $z' = z + a/2$.

forces can be identified [6, 33]. Here, we restrict ourselves to the most important contributions, the short-range chemical and exchange-correlation forces F_{chem} and the long-range vdW forces F_{vdW}, so that

$$F_{\text{ts}} = F_{\text{chem}} + F_{\text{vdW}}. \tag{2}$$

The long-range vdW forces $F_{\text{vdW}}(z)$ cannot be described within an *ab initio* calculation. Therefore, we follow suggestions in the literature for an approximate description [34]. The mesoscopic tip part is represented by a parabolic tip with curvature radius R at the height z' of the apex over the surface as depicted in figure 1(b). The resulting vdW force $F_{\text{vdW}}(z)$ between a parabolic tip and a flat surface follows the simple power law [34]

$$F_{\text{vdW}}(z') = -\frac{A_{\text{H}} R}{6 z'^2} \tag{3}$$

with the Hamaker constant A_{H}. The Hamaker constants are small and vary in the range between 10^{-19} and 10^{-20} J (see e.g. [35]). Since their variation with the interacting particles is small and the tips used in experiments are frequently coated Si ones, we use the Hamaker constant for Si–Si interaction in air [35] $A_{\text{H}} = 1.865 \times 10^{-19}$ J. The curvature radius of the parabolic tip is set to $R = 10$ nm. In order to connect the description of $F_{\text{vdW}}(z)$ to the description of $F_{\text{chem}}(z)$, we set the height of the apex of the mesoscopic tip $z' = z + a/2$, where a is the vertical extent of the microscopic pyramidal tip apex (see figure 1(b)).

2.2. Density functional theory

The short-range chemical and exchange-correlation forces are described self-consistently within spin-polarized DFT and the approximation of collinear spins. The calculations are performed

using the Vienna *ab initio* simulation package [36]. The 3d and 4s electrons of the transition-metal atoms nickel and iron as well as the 2s and 2p electrons of oxygen atoms are described as valence states. The one-particle wave functions are expanded in a basis set of plane waves up to a cutoff energy of 800 eV, whereas the projector-augmented-wave method [37] is applied to describe the wave functions in the core regions with an accuracy comparable to all-electron calculations.

In contrast to recent NiO(001) treatments including gradient corrections to the XC functional [26], here, we restrict ourselves to LDA in the parametrization of Perdew and Zunger [38]. This approach better describes the chemical forces for larger distances, for which the vdW interaction becomes important [39]. The interaction of the localized electrons on the TM 3d shell is corrected by an on-site Coulomb parameter U as demonstrated within the LDA+U method developed by Anisimov *et al* [40]. The present LDA+U calculations are based on the scheme of Dudarev *et al* [41], where only the difference between the on-site repulsion U and the exchange parameter J, U–J, enters the energy functional. Therefore, all values for U given throughout this paper are effective values representing U–J. In accordance to previous *ab initio* investigations of electronic and structural properties of the NiO bulk [32, 42] and the NiO(001) surface [26] we apply an intra-atomic d–d Coulomb energy of $U = 4$ eV to the Ni atoms. Such a U parameter opens the fundamental gap of bulk NiO [32], gives rise to a more precise magnetocrystalline anisotropy [42] and describes the properties of the NiO(001) surface properly [26]. Larger U values open the gap further [7, 8] but give rise to an incorrect energetic ordering of the electronic band structure [32]. Also to the Fe atoms in the tip, a Coulomb energy correction of $U = 4$ eV is applied for the same reasons as in the case of Ni [32].

2.3. NiO(001) surface

In the first step, we determine the equilibrium lattice constant of the antiferromagnetically ordered NiO crystal, which is represented by a rhombohedrally distorted rocksalt structure with a magnetic unit cell containing four atoms [17]. The corresponding Brillouin zone (BZ) is sampled by a mesh of $8 \times 8 \times 8$ **k**-points [43] and the internal degrees of freedom were allowed to relax until the Hellmann–Feynman forces are below 1 meV Å^{-1}. By fitting the energy versus volume curve to the Murnaghan [44] equation of state an equilibrium lattice constant of $a_0 = 4.064$ Å is obtained.

Because of the antiferromagnetic ordering AFM II the smallest lateral magnetic unit cell of the NiO(001) surface is $p(2 \times 1)$. However, both the antiferromagnetic NiO(001) surface as well as the Fe tip have to be described within the same cell. In order to avoid the lateral interaction of the Fe tips across adjacent cells, we double the size of the surface unit cell to a $p(2 \times 2)$ cell. The chosen NiO(001)2×2 surface unit cell together with the Fe tip are depicted in figure 1(a). The cell contains four formula units of NiO and can be described with basis vectors $\mathbf{a}_1 = a_0(1, 1, 0)$ and $\mathbf{a}_2 = a_0(-1, 1, 0)$. Our calculations are performed within a supercell approach, where we use symmetric slabs of five layers of NiO to represent the bulk NiO with two equivalent surfaces. Previous calculations suggest that at least nine atomic layers and a vacuum thickness of 10 Å are necessary in order to obtain well converged surface band structures [26]. However, we found that the surface energies and the forces acting on the atoms at or close to the surface converge faster with the slab thickness and are properly described with slabs of five layers. The NiO slabs are separated by a vacuum of 23 Å. This value is sufficiently large to allow the placement of the Fe tip in the vacuum such that it interacts only with one of the surfaces for the range

Table 1. Relaxation, rumpling and magnetic moments of the first two layers of the NiO(001) slab. The deviation from the bulk position in the ith layer are characterized by the rumpling R_i and the layer relaxation Δ_i in per cent of the bulk lattice constant a_0.

Layer i	R_i (%)	$\Delta_{i,i+1}$ (%)	μ_{Ni} (μ_{B})	μ_{O} (μ_{B})
1	0.89	−1.14	1.55	0.05
2	−0.79	0.01	1.53	0.03

of tip–surface distances studied in this work. Therefore, the supercell is described by the two basis vectors, $\mathbf{a}_1$ and $\mathbf{a}_2$, together with a third basis vector, $\mathbf{a}_3 = c(0, 0, 1)$ with $c = 2a_0 + 23$ Å, perpendicular to the NiO(001) surface. The corresponding BZ is sampled by a Γ-centered $4 \times 4 \times 1$ **k**-point mesh. The atomic positions of the slab are allowed to relax self-consistently until the Hellmann–Feynman forces are smaller than 1 meV Å^{-1}. The calculated values of the interlayer relaxation $\Delta_{i,i+1}$, layer rumpling R_i, as well as the local magnetic moments μ of the Ni^{2+} and O^{2-} ions in the surface and sub-surface layer are compiled in table 1. Both the calculated surface relaxation and the rumpling are small, in the order of 1%, in agreement with other available experimental and theoretical data [24, 45–50].

2.4. Fe tip and tip–surface system

The structure of the Fe tip apex that senses the short-range chemical and exchange-correlation forces is described by a cluster of five Fe atoms following [51] (see figure 1(a)). We performed several test calculations, where the tip was modeled by a single Fe atom as suggested earlier in the literature [29, 30]. However, we observed that the electronic structure of such a single Fe atom is rather unstable, most probably due to the partial occupancy of the minority-spin Fe 3d shell. In particular, magnetic moments of the tip–apex atoms as well as the tip–surface forces vary remarkably with the tip–sample distance and even change discontinuously. The tip apex modeled as a ferromagnetic five-atom iron cluster as illustrated in figure 1(a) is much more stable compared to the single Fe atom. Its shape corresponds to a pyramid of height a and a square base of length b. The orientation of the tip above the surface is chosen such that the pyramid base is parallel to the lateral basis vectors of the NiO surface $\mathbf{a}_1$ and $\mathbf{a}_2$, respectively (see figure 1(a)). The positions of the tip atoms are optimized self-consistently in absence of the NiO slab. We obtain the parameters $a = 1.69$ Å and $b = 3.38$ Å. In the five-atom cluster, the magnetic moments of the iron atoms are assumed to be ferromagnetically ordered. The lower Fe atom has a magnetic moment of $\mu_{\mathrm{Fe}} = 3.313\,\mu_{\mathrm{B}}$, while each of the four upper atoms has a slightly smaller magnetic moment of $\mu_{\mathrm{Fe}} = 3.194\,\mu_{\mathrm{B}}$. The direction of magnetization of the Fe tip determines the spin-up direction of the system of tip and surface. Ni^{2+} (and O^{2-}) ions with magnetic moments aligned parallel to the tip magnetization are, therefore, labeled Ni↑ (O↑), those aligned antiparallel are labeled Ni↓ (O↓).

The total short-range force $F_{\mathrm{chem}}(z)$ between the Fe tip and the surface is given by the sum over the Hellmann–Feynman forces acting on the tip atoms for a distance z of the Fe atom in the tip pyramid closest to the surface. At each of the eight considered lateral sites in the irreducible $p(2 \times 1)$ surface unit cell, the force $F_{\mathrm{chem}}(z)$ is calculated for tip–surface distances in the range $1.75\ \text{Å} \leqslant z \leqslant 5.00$ Å in steps of $\Delta z = 0.05$ Å which results in a total of 66 force values per site.

3. Tip–surface interaction

3.1. Forces and energies

In figure 2(a) the calculated chemical forces $F_{\mathrm{chem}}(A\sigma; z)$ acting on the Fe tip–apex at different heights $1.8 < z < 3.8$ Å above the surface atoms of species $A \in \{\mathrm{Ni}, \mathrm{O}\}$ and spin-orientation $\sigma \in \{\uparrow, \downarrow\}$ (see figure 1) are depicted. The magnetic contrast of MExFM images depends on the relative strength of the exchange forces $F_{\mathrm{X}}(A; z) = F_{\mathrm{chem}}(A\downarrow; z) - F_{\mathrm{chem}}(A\uparrow; z)$ for both species A, respectively. They are displayed in figure 2(b). Similarly, the difference in exchange (and correlation) energy $E_{\mathrm{X}} = E(A\downarrow; z) - E(A\uparrow; z)$ is obtained, where $E(A\sigma; z)$ is the total energy of the system if the Fe tip is placed at height z above the surface atom $A\sigma$. The results are plotted in figure 2(c). Negative (positive) exchange energies E_{X} indicate that the antiparallel (parallel) alignment of the magnetization of the Fe tip and the surface atom of species A is more favorable.

In figure 2(a) clear differences can be seen for the chemical forces F_{chem} acting on the tip above the different lateral sites in the surface unit cell. Above the O sites, attractive forces dominate in a wide range down to an 'equilibrium' tip–surface distance of $d_{\mathrm{Fe}\uparrow-\mathrm{O}} = 1.85$ Å with $F_{\mathrm{chem}}(\mathrm{O}\sigma; z) = 0$. There are only small differences between the forces above the two different O atoms, which can also be seen from F_{X} in figure 2(b). However, the energy difference E_{X} (figure 2(c)) reveals a weak 'antiferromagnetic' coupling ($E_{\mathrm{X}} < 0$) that might be due to superexchange interaction of the Fe tip atoms with the Ni atoms in the second layer mediated by the oxygen atoms in the surface layer [18, 19]. Above the Ni atoms, the strength of the attractive forces is smaller compared to the O sites and, consequently, the 'equilibrium' tip–surface distance is larger with $d_{\mathrm{Fe}\uparrow-\mathrm{Ni}\uparrow} = 2.1$Å ($d_{\mathrm{Fe}\uparrow-\mathrm{Ni}\downarrow} = 2.2$ Å) above the Ni↑ (Ni↓) surface atoms.

In contrast to the O sites, above the Ni sites, a contribution to the chemical forces that depends on the magnetic orientation of the Ni surface atoms relative to the tip is clearly visible in figures 2(a) and (b). Above the Ni↓ sites, the force curve is rather smooth with a maximum attraction of $F_{\mathrm{chem}} = -1.45$ nN at $z = 2.7$ Å. Above the Ni↑ sites, however, the situation is more complex. While for tip–surface distances larger than $z = 2.7$ Å, the attractive forces above the Ni↑ sites are smaller compared to the Ni↓ sites, the situation is reversed below $z = 2.7$ Å and, hence, the exchange force $F_{\mathrm{X}}(\mathrm{Ni})$ in figure 2(a) changes its sign. The appearance of an additional attractive force on the Fe tip above the Ni↑ sites for tip–surface distances smaller than $z = 2.7$ Å coincides also with the minimum of $E_{\mathrm{X}}(\mathrm{Ni})$. From figure 2(c) it becomes clear, that above $z = 2.7$ Å the antiferromagnetic coupling between tip and surface is most important and stabilized with decreasing tip–surface distance. Below $z = 2.7$ Å an opposite contribution to E_{X} appears and the parallel configuration between tip and surface Ni atoms is stabilized compared to the antiparallel configuration. The parallel configuration becomes the favorable configuration below $z = 2.3$ Å for the tip above the Ni sites.

Our results agree roughly with those of Momida and Oguchi [30], where the tip was modeled by only one Fe atom and no U correction was considered. However, a detailed comparison of the results is not possible. Due to the few sampling points and the fitting procedure used in their study, their force versus distance curves are smooth functions throughout the whole range of heights studied. Most importantly, the sharp change of the interaction at a height $z = 2.7$ Å above the Ni↑ atom is not visible in their force curves.

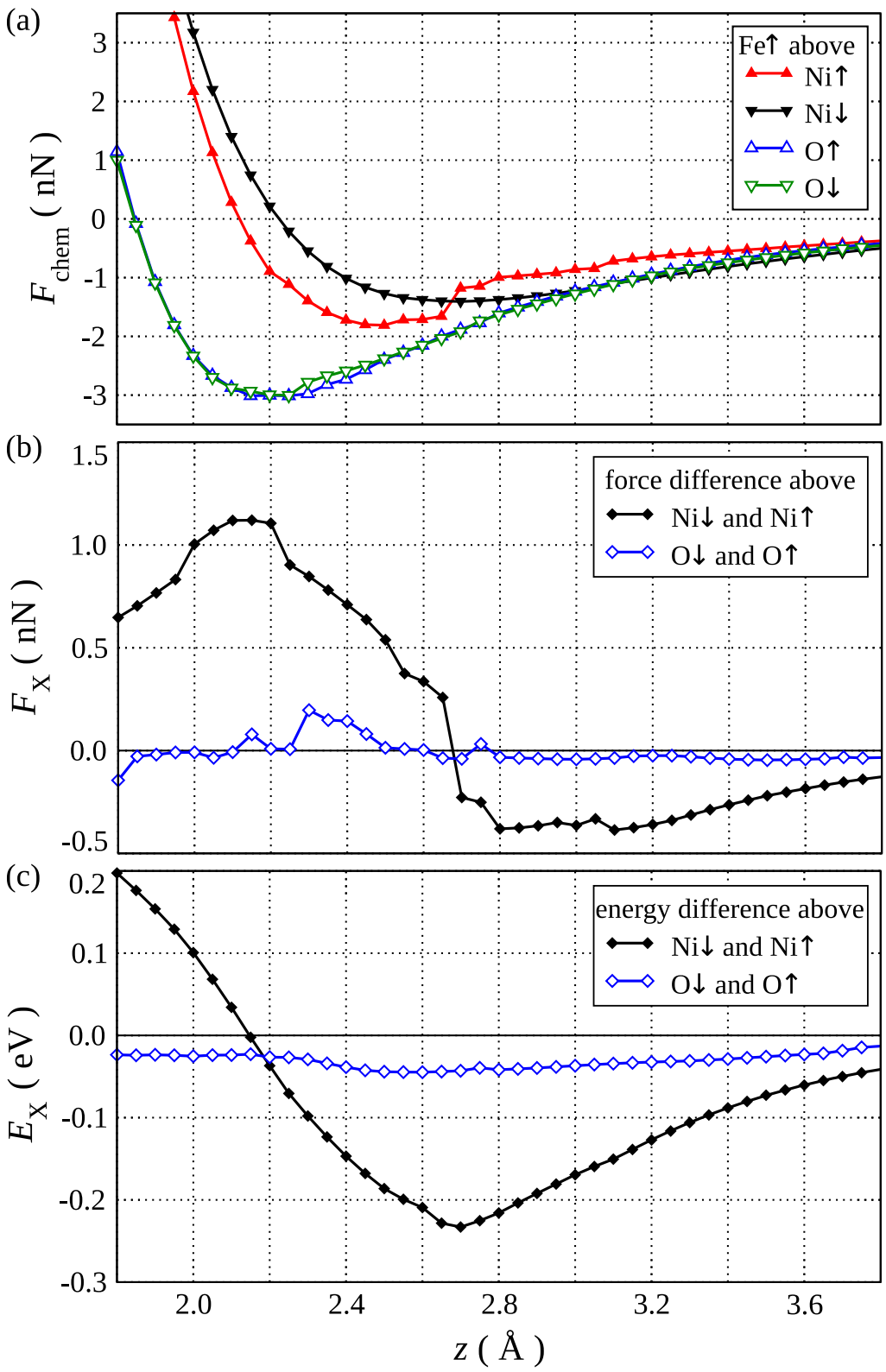

Figure 2. (a) Chemical forces F_{chem}, (b) exchange forces F_X and (c) exchange energies E_X at the lateral position of the four surface atoms in the 2×1 unit cell versus the tip–surface distance z.

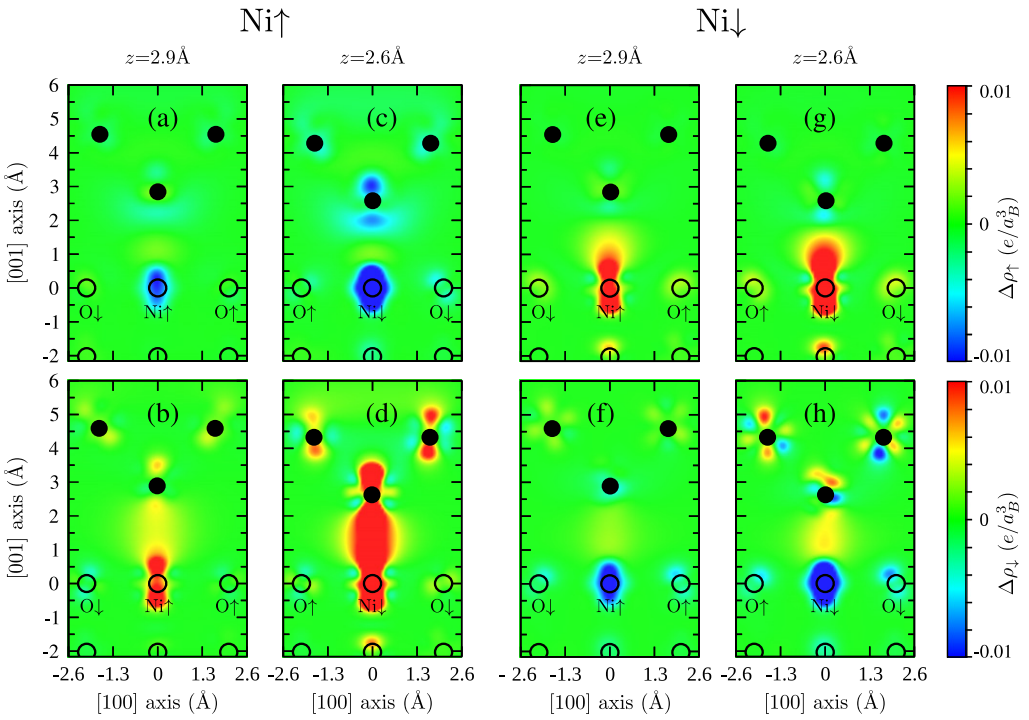

Figure 3. Changes of the spin densities $\Delta\rho^\sigma$ in the (010) plane due to tip–surface interaction. The upper (lower) panels show the variation in the spin-up channel $\Delta\rho^\uparrow$ (spin-down channel $\Delta\rho^\downarrow$). Black dots indicate Fe tip atoms, while open circles represent Ni and O atoms in the first two slab layers. The tip is positioned above the two surface atoms Ni↑ ((a)–(f)) and Ni↓ ((e)–(h)) for two different tip heights $z = 2.9$ Å ((a), (b), (e) and (f)) and $z = 2.6$ Å ((c), (d), (g) and (h)). Positive values (red areas) indicate an accumulation and negative values (blue areas) a depletion of spin density caused by the tip–surface interaction.

3.2. Redistribution of spin-polarized electrons

In order to understand the mechanisms that determine the tip–surface interaction, we investigate the change of the spin densities $\Delta\rho^\sigma = \rho^\sigma_{\mathrm{ts}} - \rho^\sigma_{\mathrm{t}} - \rho^\sigma_{\mathrm{s}}$ due to the interaction, where $\rho^\sigma_{\mathrm{ts}}$ is the spin-density component σ of the interacting system and ρ^σ_{t} and ρ^σ_{s} are the spin densities of the non-interacting tip and slab, respectively. In figure 3 $\Delta\rho^\sigma$ is depicted in the (010) plane with the tip apex at two different heights, $z = 2.6$ and 2.9 Å, i.e. above and below the critical distance of $z = 2.7$ Å, above the Ni↑ and Ni↓ atoms. For the chosen Fe tip the spin-up (spin-down) channel in figure 3 corresponds to the majority-(minority-)spin channel. While for the Ni↑ atom (figures 3(a)–(d)) the spin-orientation is the same as for the Fe tip atoms, the situation is reversed for the Ni↓ atom (figures 3(e)–(h)). In particular, the spin-up (spin-down) channel corresponds to the minority-(majority-)spin channel for the Ni↓ atom.

At the chosen heights, we observe that the presence of the ferromagnetic tip leads to a rather strong redistribution of the spin densities in a d_{z^2} state at the Ni surface atoms. In particular, we find an increased density in the minority-spin d_{z^2} state of the Ni surface atoms (figures 3(b), (d), (e) and (g)), whereas the density of the majority-spin d_{z^2} state of the Ni atoms decreases (figures 3(a), (c), (f) and (h)). Interestingly, the redistribution of spin density at the Ni atoms appears to be rather independent of the alignment of the magnetic moments with respect to the

ferromagnetic tip. For the Fe atoms in the tip, the situation is more complicated and the actual redistribution depends on both the height and whether the tip is located above the Ni↑ or Ni↓ atom. At the height $z = 2.9$ Å (figures 3(a), (b), (e) and (f)), we find no redistribution of the Fe majority-spin electrons (figures 3(a) and (e)) and only a very weak redistribution of the minority-spin electrons (figures 3(b) and (f)) above both Ni atoms. This, however, changes drastically at the smaller distance $z = 2.6$ Å. Above the Ni↓ atom (figures 3(g) and (h)) the Fe majority-spin electrons remain unpolarized (figure 3(g)), whereas we observe some redistribution of electrons within the Fe minority-spin channel with a small accumulation of electron density between the tip apex and the surface (figure 3(h)). In contrast, above the Ni↑ atom (figures 3(c) and (d)), the changes are much stronger. Similar to the Ni atoms, we observe a strong redistribution of the electron density in a d_{z^2} state of the Fe atom at the tip apex. Also, here the minority-spin density of the d_{z^2} state increases (figure 3(d)), whereas the majority-spin density of the d_{z^2} state decreases (figure 3(c)). It is evident from figure 3(d) that above the Ni↑ atom at heights below the critical height $z = 2.7$ Å (i) a strong redistribution of spin density at the Fe atom at the tip apex takes place and (ii) some covalent bond between minority-spin electrons in d_{z^2} like states of the Ni↑ atom and the Fe atom at the tip apex is formed. Obviously, the presence of this covalent bond causes both the additional attractive force on the Fe tip above the Ni↑ atom observed in figures 2(a) and (b) as well as the additional ferromagnetic coupling visible in figure 2(c).

3.3. Interaction mechanisms

The differences in the chemical forces $F_{\mathrm{chem}}(z)$ (see figure 2) acting on the cores of the Fe atoms at the tip apex, above the surface Ni and O ions with opposite ionic charges as well as that between Ni ions with opposite spin moment indicate two leading mechanisms. The first one is of electrostatic nature. It is due to the interaction of the Fe atoms with the electrostatic field caused by the oppositely charged ions in the NiO surface. At tip–surface distances z larger than a characteristic distance of 3 Å (see figure 2), that is of the order of nearest-neighbor distances in Fe and Ni metals but somewhat larger than the nearest-neighbor distance in FeO, the electrostatic fields of the oppositely charged ions in the NiO surface tend to cancel each other. Hence, the action of the total electrostatic field caused by the slab of ions and, hence, its contribution to the Hellmann–Feynman forces vanishes. However, this picture changes drastically for small distances $z < 3$ Å. In this region, the local electrostatic field of the closest probed surface ion becomes most important. The strongest interaction happens with the tip–apex Fe atom that is differently polarized in dependence on the tip position above a Ni or O ion. The core of the Fe atom at the tip apex is attracted (repelled) by the negatively (positively) charged O^{2-} (Ni^{2+}) ions. This explains why the chemical forces $F_{\mathrm{chem}}(z)$ acting on the tip are significantly larger above the O^{2-} ions compared to the Ni^{2+} ions. Similar results regarding the stronger attraction of metallic tips above anion sites compared to cation sites have been reported also for non-magnetic AFM experiments, where a chromium tip was used to probe the surface of sodium chloride [52].

The second important contribution to the Hellmann–Feynman forces $F_{\mathrm{chem}}(z)$ stems from the redistribution of the spin electron densities in the vicinity of the Fe atom at the tip apex and the surface ion underneath (see figure 3). Even the formation of some bonds, as in the case shown in figure 3(d), may occur. Such a contribution leads to an attractive force on the tip. Most importantly, these redistributions, figure 3, depend significantly on the distance, the spin channel and the spin of the Ni surface ions. Therefore, the forces due to bond formation are also responsible for the crossing of the $F_{\mathrm{chem}}(z)$ curves above the Ni↑ and Ni↓ atoms at $z = 2.7$ Å

(see figure 2). If the tip is located above the Ni↓ atom, the electron density of the atom at the tip apex remains almost unchanged (see figures 3(e)–(h)). Primarily, the redistribution of spin density from the majority Ni d_{z^2} into the minority Ni d_{z^2} increases the electron density between tip and surface and, hence, the attractive force on the tip is relatively small. Above the Ni↑ atom, the situation is different. For $z = 2.9$ Å, only a small amount of minority-spin density is accumulated between the tip and the Ni↑ atom (see figure 3(b)). Consequently, the attractive force on the tip is small. This behavior changes drastically for distances $z < 2.7$ Å, visible in figure 3(d) for $z = 2.6$ Å. Below $z < 2.7$ Å the bond formation between the minority-spin electrons of the tip and the Ni↑ atom leads to a large displacement of valence electrons and, hence, a strong attractive contribution to the Hellmann–Feynman forces.

In order to understand the bonding or non-bonding mechanisms above the Ni↑ and Ni↓ atoms more deeply, we focus on the interaction of the spin-dependent orbitals of the closest tip–apex Fe atom and the Ni↑ and Ni↓ surface ions. For the tip above the Ni↓ atom, the electrons in the d_{z^2} states of the Fe tip atom and the Ni↓ atom belong to different spin channels. Therefore, direct exchange interaction is not possible. The Coulomb repulsion of electrons with opposite spin at the two transition-metal atoms also prevents the formation of a symmetric covalent bond with spin-paired electrons. Consequently, the interaction between the Fe tip and the Ni↓ atom is best described by the kinetic exchange mechanism according to Anderson [18, 19, 53]. This mechanism is also expressed in the Kanamori–Goodenough rule [54, 55] for the interaction between magnetic cations, which states that the interaction between two half-filled localized orbitals located at different cations should be antiferromagnetic.

For the tip above the Ni↑ atom we identify two different mechanisms depending on the tip–surface distance. At large distances $z > 2.7$ Å, the d_{z^2} electrons of the tip Fe atom and the Ni↑ atom are localized at the respective atom. Since both of them belong to the same spin channel their interaction may be described by a direct Heitler–London exchange [56]. At intermediate distances, the formation of spin-dependent molecular orbitals occurs. The unoccupied bonding ddσ minority-spin molecular orbital is shifted toward lower energies and becomes occupied below $z = 2.7$ Å (see figure 3(d)). It is accompanied by an energy gain. This bond formation has two consequences: (i) the ferromagnetic coupling between Fe tip and the Ni↑ atoms, e.g. visible in the energy in figure 2(c), is stabilized and (ii) the redistribution of electron density from the interacting atoms into the bonding region leads to an additional attractive contribution to the force F_{chem} in figures 2(a) and (b). The observed mechanism might be related to the 'covalent magnetism' reported earlier [57]. It is also interesting to note that Goodenough [56, 58] pointed out the importance of a critical atomic separation of 2.9 Å for the interaction in transition metals and their alloys, above which the electrons behave strongly localized and below where bond and band formation appear.

4. Simulation of MExFM

MExFM images are obtained by plotting the corrugation height over the surface unit cell. We choose the minimum tip–surface distance above the Ni↓ atom $d(\gamma; \mathrm{Ni}\downarrow)$ as the reference for this height $\Delta d(\gamma; x, y) = d(\gamma; x, y) - d(\gamma; \mathrm{Ni}\downarrow)$. We further introduce the average chemical corrugation

$$\Delta d_{\mathrm{chem}}(\gamma) = \frac{1}{2} \sum_{\sigma} \{\Delta d(\gamma; \mathrm{O}\sigma) - \Delta d(\gamma; \mathrm{Ni}\sigma)\} \tag{4}$$

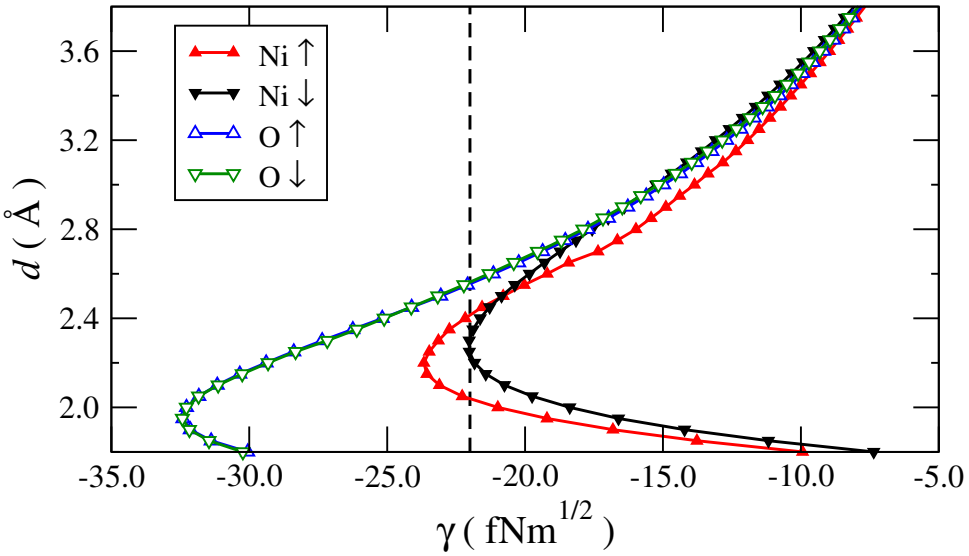

Figure 4. Minimal tip–surface distance d as a function of the normalized frequency shift γ for tip positions above the four surface atoms of the NiO(001)2×1 surface unit cell. The limiting frequency shift for the calculation of MExFM images $\gamma_{\max}$ is indicated by the dashed line.

as well as the magnetic corrugation between the two Ni atoms, i.e. the spin contrast

$$\Delta d_{\mathrm{Ni}}(\gamma) = \Delta d(\gamma; \mathrm{Ni}\uparrow) - \Delta d(\gamma; \mathrm{Ni}\downarrow). \tag{5}$$

The functions $d(\gamma; x, y)$ for the Fe tip above the four different surface atoms are plotted in figure 4 versus the normalized frequency shift γ. We recognize that $\gamma(d; x, y)$ versus d follows the trend of the chemical forces. However, compared to figure 2(a), the curves in figure 4 are smoother and shifted toward lower heights as a result of the integration and the inclusion of attractive vdW forces. From figure 4 it is evident, that the largest possible frequency shift for the calculation of MExFM images in our model is $\gamma_{\max} = -22.1\,\mathrm{fN\,m^{1/2}}$. It is obtained if the oscillating Fe tip is placed above the Ni↓ atom with a minimum tip–surface distance of $d = 2.3$ Å. Further reduction of the minimum tip–surface distance above this site brings the tip into the repulsive regime of the tip–surface interaction, which effectively reduces the average force over one oscillation cycle and, hence, leads to a reduced frequency shift. Since MExFM experiments are performed at tip–surface distances where the tip–surface interaction is attractive, we will restrict our discussion to this regime as well.

For small frequency shifts $-18\,\mathrm{fN\,m^{1/2}} < \gamma$, the splitting in figure 4 between the $d(\gamma)$ curves is generally rather small. We observe that there is a certain splitting between the $d(\gamma)$ curves calculated above the two Ni atoms, while the $d(\gamma)$ curves obtained above the two O atoms coincide with the $d(\gamma)$ curve above the Ni↓ atom. Consequently, some magnetic contrast is visible between the two Ni atoms, while no contrast is visible between the Ni↓ atom and the two O atoms. Both the chemical corrugation $\Delta d_{\mathrm{chem}}(\gamma)$ and the magnetic corrugation $\Delta d_{\mathrm{Ni}}(\gamma)$ remain small with values of 6 and 12 pm, respectively. In the range $-22.1 < \gamma < -18.0\,\mathrm{fN\,m^{1/2}}$, the splittings between the $d(\gamma)$ curves change drastically. In the interval $-21.0 < \gamma < -18\,\mathrm{fN\,m^{1/2}}$, the chemical corrugation $\Delta d_{\mathrm{chem}}(\gamma)$ increases from around 7 to 13 pm, while the magnetic corrugation $\Delta d_{\mathrm{Ni}}(\gamma)$ decreases from around 9 pm and vanishes at

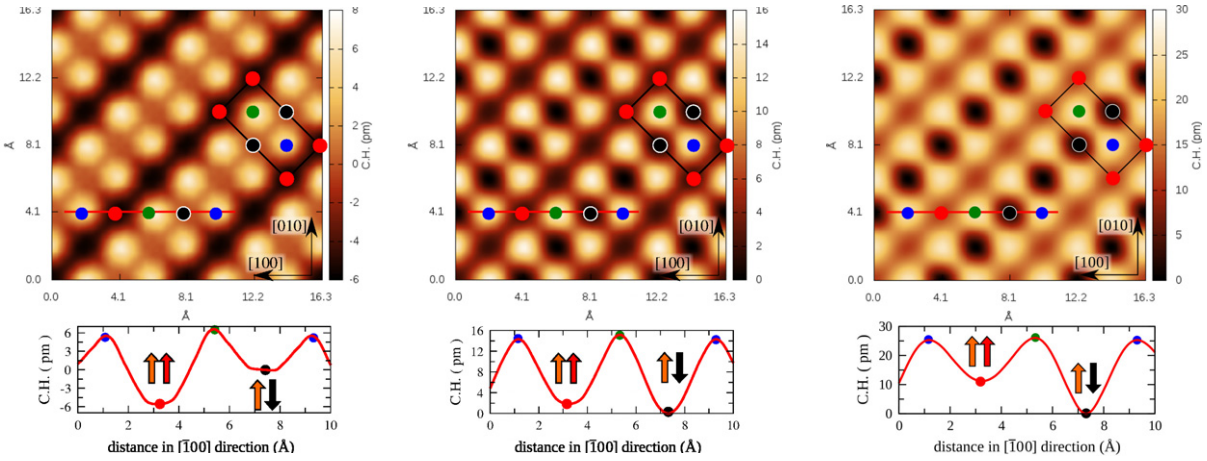

Figure 5. Calculated MExFM images at three different frequency shifts (a) $\gamma = -19.3\,\mathrm{fN\,m^{1/2}}$, (b) $\gamma = -21.3\,\mathrm{fN\,m^{1/2}}$ and (c) $\gamma = -22.0\,\mathrm{fN\,m^{1/2}}$. A $p(2 \times 1)$ surface unit cell is indicated by a rectangle. The colors of the surface unit cell are the same as in figure 1(a). The plots below represent the line profile indicated by the red lines in the MExFM images. Orange and red (black) arrows indicate the spin alignment between Fe↑ and Ni↑ (Ni↓).

$\gamma = -21.0\,\mathrm{fN\,m^{1/2}}$. Corresponding MExFM images are calculated for the frequency shifts $\gamma = -19.3$ and $-21.3\,\mathrm{fN\,m^{1/2}}$ and depicted in figures 5(a) and (b). The vanishing magnetic contrast around $\gamma = -21.0\,\mathrm{fN\,m^{1/2}}$ visible in figure 5(b) is a direct consequence of the crossing of the $F_{\mathrm{chem}}(z)$ curves above the two Ni atoms discussed earlier. For $-22.1 < \gamma < -21.0\,\mathrm{fN\,m^{1/2}}$ both the chemical and the magnetic corrugations increase and become large close to the critical frequency shift $\gamma_{\mathrm{max}} = -22.1\,\mathrm{fN\,m^{1/2}}$. The average chemical corrugation $\Delta d_{\mathrm{chem}}(\gamma)$ increases to about 20 pm and the magnetic corrugation $\Delta d_{\mathrm{Ni}}(\gamma)$ increases to about 11 pm slightly below the critical frequency shift $\gamma_{\mathrm{max}} = -22.1\,\mathrm{fN\,m^{1/2}}$. A corresponding MExFM image is shown in figure 5(c) for $\gamma = -22.0\,\mathrm{fN\,m^{1/2}}$.

Our results can be compared to the experimental investigations of Kaiser *et al* [13], where two MExFM images were obtained at frequency shifts corresponding to $\gamma = -2.6$ and $-2.7\,\mathrm{fN\,m^{1/2}}$. While the image taken at $\gamma = -2.6\,\mathrm{fN\,m^{1/2}}$ shows only a chemical corrugation $\Delta d_{\mathrm{chem}} \approx 4.5$ pm, the other image obtained at a slightly higher frequency shift $\gamma = -2.7\,\mathrm{fN\,m^{1/2}}$ shows both chemical corrugation $d_{\mathrm{chem}} \approx 4.5$ pm and a weaker magnetic corrugation $\Delta d_{\mathrm{Ni}} \approx 1.5$ pm [13]. Our calculated MExFM images as well as the corresponding line profiles in figures 5(b) and (c) agree qualitatively very well with the results of Kaiser *et al* (figures 2(a) and (b) in [13]). In particular, the fact that we obtain vanishing magnetic contrast between the Ni atoms while the chemical contrast is retained at a certain frequency shift in figure 5(b) is noteworthy. In our calculations, this effect can be traced back to the crossing of the force versus height curves in figure 2 above the Ni atoms, which is related to the formation of a bond between d_{z^2} -like states in the minority-spin channel of the Ni↑ and the Fe atom at the tip apex. This effect might explain why Kaiser *et al* [13] could not observe magnetic contrast at the lower frequency shift but only at a somewhat larger frequency shift, despite the otherwise identical experimental setup with a strong magnetic field in order to magnetize the Fe coated tip.

In a recent experiment, Pielmeier and Giessibl [14] performed MExFM measurements on the NiO(001) surface using a Fe tip, but in contrast to the experiment of Kaiser *et al* [13] without

an external magnetic field to magnetize the tip. In their experiment, Pielmeier and Giessibl [14] observe only a weak magnetic contrast if the Fe tip is located above the O ions, which they relate to superexchange interaction of the Fe tip atom with the magnetic Ni ions in the first sub-surface layer. Such magnetic contrast above the O ions is also present in our calculations, however, it is small compared to the magnetic contrast above the Ni ions. Nevertheless, at the frequency shift $\gamma \approx 21\,\mathrm{fN\,m^{1/2}}$ (see figure 4), where the magnetic contrast between the Ni↑ and Ni↓ ions vanishes, the magnetic contrast above the O ions remains (see line plot in figure 5(b)). These facts can be considered as a qualitative interpretation of the findings of Pielmeier and Giessibl [14].

However, we have to state that the absolute values of frequency shifts γ and the calculated corrugations $\Delta d_{\mathrm{chem}}(\gamma)$ and $\Delta d_{\mathrm{Ni}}(\gamma)$, are much larger compared to the experimental values of Kaiser *et al* [13] or Pielmeier and Giessibl [14]. Nevertheless, the ratio $\Delta d_{\mathrm{chem}}/\Delta d_{\mathrm{Ni}} \approx 2$ in our calculations and $\Delta d_{\mathrm{chem}}/\Delta d_{\mathrm{Ni}} \approx 3$ in the measurements of Kaiser *et al* [13] are very close to each other. Some factors may explain the discrepancies between the calculated and the measured absolute values: (i) the experimentally obtained corrugation heights depend on the actual experimental setup. In other NC-AFM investigations of the NiO(001) surface a wide range of corrugations of up to 40–50 pm are measured [5, 14, 59–62]. Our calculated results are well below such large values. (ii) The vdW forces are treated within a simple model with certain assumptions about the Hamaker constant and the tip shape. A more sophisticated approach could also include vdW interaction directly in an *ab initio* method, e.g. in the framework of the adiabatic-connection fluctuation-dissipation theorem [63]. (iii) We did not allow for atomic relaxation of the surface and the tip due to their interaction. Theoretical studies of other systems [51, 64] suggest that the inclusion of relaxation may have a strong influence on resulting forces and especially on their distance dependence. Indeed, Kaiser *et al* [65] predicted a strong relaxation influence for the MExFM on NiO(001).

Nevertheless, we have to point out the power of the present description compared to previous theoretical studies [30]. They predict the largest corrugation between the two Ni atoms while the O atoms show only intermediate corrugation with respect to the Ni atoms. This is clearly in conflict with our results and the experimental data of Kaiser *et al* [13]. Therefore, we claim that not only the improved description of the tip apex by a pyramid of five Fe atoms and the higher sampling of the forces at various distances, but also the inclusion of vdW interaction and the accurate calculation of the frequency shift according to (1) are essential for the predictive power of the presented theory for magnetic images.

5. Summary and conclusions

We have presented *ab initio* calculations of the quantum-mechanical interactions between the surface of a substrate with magnetic ordering and a ferromagnetic tip. The antiferromagnetic NiO(001)2×1 surface together with an iron tip have been considered as prototypical examples. The tip apex has been modeled as a pyramid of five ferromagnetically aligned Fe atoms. The chemical forces, calculated within an *ab initio* approach, are combined with an empirical description of the vdW forces between the surface and the more distant parts of the tip.

The chemical and magnetic exchange forces and energies have been studied as functions of the tip–surface separation and the lateral position of the tip. In agreement with experiments, we observe larger attractive chemical forces if the Fe tip is located above the negatively charged oxygen ions rather than above the positively charged nickel ions. The reason for this is the

electrostatic attraction (repulsion) of the core of the Fe atom at the tip apex closest to the surface above the negatively (positively) charged ions. An interplay of different interaction mechanisms is responsible for the magnetic contrast between the surface Ni ions. In the long-distance regime, the chemical forces are dominated by kinetic exchange while, for small distances, spin-dependent covalent bonding appears. The drastic changes in the tip–surface interaction, below a critical tip–surface distance, are explained by the bond formation between the Fe tip and the Ni↑ atoms, which leads to an additional attractive force and, hence, causes a crossing of the force versus distance curves above the two Ni atoms. The corresponding exchange energy favors an antiparallel spin alignment between the tip apex and the closest probed surface Ni ion above the critical distance and a parallel spin alignment at small distances. The spin alignment of the oxygen atoms is less important.

The simulated MExFM images and corrugation heights along high-symmetry directions are in good qualitative agreement with recent experimental studies. In particular, the presented theoretical description shows how and why magnetic contrast is obtained at a certain frequency shift, while it vanishes at slightly smaller ones. The presented theory possesses a predictive power for the contrast pattern over the entire surface unit cell but especially for the contrast between the magnetic ions. The absolute values of normalized frequency shifts and corrugation heights are, however, overestimated. Even though earlier force microscopy studies indicated the possibility of corrugation heights in the order of magnitude obtained here, we believe that further improvements of the simulation should be made. Critical are the tip size and the description of the vdW interaction. The inclusion of atomic relaxation due to tip–surface interaction and a description of the electronic and magnetic phenomena including spin–orbit interaction may also improve the quantitative description.

Acknowledgments

We acknowledge financial support by the Deutsche Forschungsgemeinschaft within the research training group GRK 1523 ‘Quantum and Gravitational Fields’ of the Friedrich–Schiller Universität Jena and the project Be1346/20-1.

References

[1] Khajetoorians A A, Wiebe J, Chilian B and Wiesendanger R 2011 Realizing all-spin-based logic operations atom by atom *Science* **332** 1062–4

[2] Khajetoorians A A *et al* 2013 Current-driven spin dynamics of artificially constructed quantum magnets *Science* **339** 55–9

[3] Pierce D T 1988 Spin-polarized electron microscopy *Phys. Scr.* **38** 291

[4] Wiesendanger R, Güntherodt H-J, Güntherodt G, Gambino R J and Ruf R 1990 Observation of vacuum tunneling of spin-polarized electrons with the scanning tunneling microscope *Phys. Rev. Lett.* **65** 247–50

[5] Sueoka K, Subagyo A, Hosoi H and Mukasa K 2004 Magnetic imaging with scanning probe microscopy *Nanotechnology* **15** S691

[6] Wiesendanger R 2009 Spin mapping at the nanoscale and atomic scale *Rev. Mod. Phys.* **81** 1495–550

[7] Castell M R, Wincott P L, Condon N G, Muggelberg C, Thornton G, Dudarev S L, Sutton A P and Briggs G A D 1997 Atomic-resolution STM of a system with strongly correlated electrons: NiO(001) surface structure and defect sites *Phys. Rev.* B **55** 7859–63

[8] Castell M R, Dudarev S L, Briggs G A D and Sutton A P 1999 Unexpected differences in the surface electronic structure of NiO and CoO observed by STM and explained by first-principles theory *Phys. Rev.* B **59** 7342–5

[9] Heike S, Wada Y, Kondo S, Lutwyche M, Murayama K and Kuroda H 1994 Scanning tunneling microscope measurement of insulator surfaces *Appl. Phys. Lett.* **64** 1100–2
[10] Binnig G, Quate C F and Gerber Ch 1986 Atomic force microscope *Phys. Rev. Lett.* **56** 930–3
[11] Wiesendanger R, Bürgler D, Tarrach G, Schaub T, Hartmann U, Güntherodt H-J, Shvets I V and Coey J M D 1991 Recent advances in scanning tunneling microscopy involving magnetic probes and samples *Appl. Phys.* A **53** 349–55
[12] Mukasa K, Hasegawa H, Tazuke Y, Sueoka K, Sasaki M and Hayakawa K 1994 Exchange interaction between magnetic moments of ferromagnetic sample and tip: possibility of atomic-resolution images of exchange interactions using exchange force microscopy *Japan. J. Appl. Phys.* **33** 2692–5
[13] Kaiser U, Schwarz A and Wiesendanger R 2007 Magnetic exchange force microscopy with atomic resolution *Nature* **446** 522–5
[14] Pielmeier F and Giessibl F J 2013 Spin resolution and evidence for superexchange on NiO(001) observed by force microscopy *Phys. Rev. Lett.* **110** 266101
[15] Schmidt R, Lazo C, Hölscher H, Pi U H, Caciuc V, Schwarz A, Wiesendanger R and Heinze S 2009 Probing the magnetic exchange forces of iron on the atomic scale *Nano Lett.* **9** 200–4
[16] Duo L, Finazzi M and Ciccacci F 2010 *Magnetic Properties of Antiferromagnetic Oxide Materials: Surfaces, Interfaces and Thin Films* (New York: Wiley)
[17] Roth W L 1958 Magnetic structures of MnO, FeO, CoO and NiO *Phys. Rev.* **110** 1333–41
[18] Anderson P W 1959 New approach to the theory of superexchange interactions *Phys. Rev.* **115** 2–13
[19] Anderson P W 1963 Theory of magnetic exchange interactions: exchange in insulators and semiconductors *Solid State Phys.* **14** 99–214
[20] Kittel C 2005 *Introduction to Solid State Physics* (New York: Wiley)
[21] Hohenberg P and Kohn W 1964 Inhomogeneous electron gas *Phys. Rev.* **136** B864–71
[22] Kohn W and Sham L J 1965 Self-consistent equations including exchange and correlation effects *Phys. Rev.* **140** A1133–8
[23] Dudarev S L, Liechtenstein A I, Castell M R, Briggs G A D and Sutton A P 1997 Surface states on NiO(100) and the origin of the contrast reversal in atomically resolved scanning tunneling microscope images *Phys. Rev.* B **56** 4900–8
[24] Momida H and Oguchi T 2002 First-principles studies of antiferromagnetic MnO and NiO surfaces *J. Phys. Soc. Japan* **72** 588–93
[25] Ködderitzsch D, Hergert W, Temmerman W M, Szotek Z, Ernst A and Winter H 2002 Exchange interactions in NiO and at the NiO(100) surface *Phys. Rev.* B **66** 064434
[26] Schrön A, Granovskij M and Bechstedt F 2013 Influence of on-site Coulomb interaction U on properties of MnO(001)2 × 1 and NiO(001)2 × 1 surfaces *J. Phys.: Condens. Matter* **25** 094006
[27] Schwarz A, Kaiser U and Wiesendanger R 2009 Towards an understanding of the atomic scale magnetic contrast formation in NC-AFM: a tip material dependent MExFM study on NiO(001) *Nanotechnology* **20** 264017
[28] Lazo C and Heinze S 2011 First-principles study of magnetic exchange force microscopy with ferromagnetic and antiferromagnetic tips *Phys. Rev.* B **84** 144428
[29] Foster A S and Shluger A L 2001 Spin-contrast in non-contact SFM on oxide surfaces: theoretical modelling of NiO(001) surface *Surf. Sci.* **490** 211–9
[30] Momida H and Oguchi T 2005 First-principles study on exchange force image of NiO(001) surface using a ferromagnetic Fe probe *Surf. Sci.* **590** 42–50
[31] Tran F, Blaha P, Schwarz K and Novàk P 2006 Hybrid exchange-correlation energy functionals for strongly correlated electrons: applications to transition-metal monoxides *Phys. Rev.* B **74** 155108
[32] Rödl C, Fuchs F, Furthmüller J and Bechstedt F 2009 Quasiparticle band structures of the antiferromagnetic transition-metal oxides MnO, FeO, CoO and NiO *Phys. Rev.* B **79** 235114
[33] García R and Pérez R 2002 Dynamic atomic force microscopy methods *Surf. Sci. Rep.* **47** 197–301
[34] Giessibl F J 1997 Forces and frequency shifts in atomic-resolution dynamic-force microscopy *Phys. Rev.* B **56** 16010–5

[35] Bergström L 1997 Hamaker constants of inorganic materials *Adv. Colloid Interface Sci.* **70** 125–69
[36] Kresse G and Furthmüller J 1996 Efficiency of *ab initio* total energy calculations for metals and semiconductors using a plane-wave basis set *Comput. Mater. Sci.* **6** 15–50
[37] Kresse G and Joubert D 1999 From ultrasoft pseudopotentials to the projector augmented-wave method *Phys. Rev.* B **59** 1758
[38] Perdew J P and Zunger A 1981 Self-interaction correction to density-functional approximations for many-electron systems *Phys. Rev.* B **23** 5048–79
[39] Ortmann F, Schmidt W G and Bechstedt F 2005 Attracted by long-range electron correlation: adenine on graphite *Phys. Rev. Lett.* **95** 186101
[40] Anisimov V I, Zaanen J and Andersen O K 1991 Band theory and Mott insulators: Hubbard U instead of Stoner I *Phys. Rev.* B **44** 943–54
[41] Dudarev S L, Botton G A, Savrasov S Y, Szotek Z, Temmerman W M and Sutton A P 1998 Electronic structure and elastic properties of strongly correlated metal oxides from first principles: LSDA + U, SIC-LSDA and EELS study of UO_2 and NiO *Phys. Status Solidi* **166** 429–43
[42] Schrön A, Rödl C and Bechstedt F 2012 Crystalline and magnetic anisotropy of the 3d-transition metal monoxides MnO, FeO, CoO and NiO *Phys. Rev.* B **86** 115134
[43] Monkhorst H J and Pack J D 1976 Special points for Brillouin-zone integrations *Phys. Rev.* B **13** 5188–92
[44] Murnaghan F D 1944 The compressibility of media under extreme pressures *Proc. Natl Acad. Sci. USA* **30** 244
[45] Welton-Cook M R and Prutton M 1980 Leed calculations for the NiO(100) surface: extension to lower energies *J. Phys. C: Solid State Phys.* **13** 3993
[46] Yikegaki T, Shibata H, Takatoh S, Fujikawa T and Usami S 1990 Study on surface structure by grazing incidence EELFS *Phys. Scr.* **41** 185
[47] Okazawa T, Yagi Y and Kido Y 2003 Rumpled surface structure and lattice dynamics of NiO(001) *Phys. Rev.* B **67** 195406
[48] Okazawa T, Nakagawa Y and Kido Y 2004 Temperature-dependent surface structure and lattice dynamics of NiO(001) *Phys. Rev.* B **69** 125412
[49] Rohrbach A, Hafner J and Kresse G 2004 Molecular adsorption on the surface of strongly correlated transition-metal oxides: a case study for CO/NiO(100) *Phys. Rev.* B **69** 075413
[50] Yu N, Zhang W-B, Wang N, Wang Y-F and Tang-Yu B 2008 Water adsorption on a NiO(100) surface: a GGA + U study *J. Phys. Chem.* C **112** 452–7
[51] Lazo C, Caciuc V, Hölscher H and Heinze S 2008 Role of tip size, orientation and structural relaxations in first-principles studies of magnetic exchange force microscopy and spin-polarized scanning tunneling microscopy *Phys. Rev.* B **78** 214416
[52] Teobaldi G, Lämmle K, Trevethan T, Watkins M, Schwarz A, Wiesendanger R and Shluger A L 2011 Chemical resolution at ionic crystal surfaces using dynamic atomic force microscopy with metallic tips *Phys. Rev. Lett.* **106** 216102
[53] Palii A, Tsukerblat B, Clemente-Juan J M and Coronado E 2010 Magnetic exchange between metal ions with unquenched orbital angular momenta: basic concepts and relevance to molecular magnetism *Int. Rev. Phys. Chem.* **29** 135–230
[54] Goodenough J B 1963 *Magnetism and the Chemical Bond* vol 98 (New York: Interscience)
[55] Kugel' K I and Khomskii D I 1982 The Jahn–Teller effect and magnetism: transition metal compounds *Sov. Phys.—Usp.* **25** 231
[56] Goodenough J B 1960 Band structure of transition metals and their alloys *Phys. Rev.* **120** 67–83
[57] Williams A R, Zeller R, Moruzzi V L, Gelatt C D and Kubler J 1981 Covalent magnetism: an alternative to the Stoner model *J. Appl. Phys.* **52** 2067–9
[58] Goodenough J B 1960 Direct cation–cation interactions in several oxides *Phys. Rev.* **117** 1442–51
[59] Langkat S M 2002 Tieftemperatur-Rasterkraftmikroskopie auf antiferromagnetischen Übergangsmetalloxiden *PhD Thesis* Universität Hamburg
[60] Hölscher H, Langkat S M, Schwarz A and Wiesendanger R 2002 Measurement of three-dimensional force fields with atomic resolution using dynamic force spectroscopy *Appl. Phys. Lett.* **81** 4428–30

[61] Langkat S M, Hölscher H, Schwarz A and Wiesendanger R 2003 Determination of site specific interatomic forces between an iron coated tip and the NiO(001) surface by force field spectroscopy *Surf. Sci.* **527** 12–20
[62] Schmid M, Mannhart J and Giessibl F J 2008 Searching atomic spin contrast on nickel oxide (001) by force microscopy *Phys. Rev.* B **77** 045402
[63] Harl J and Kresse G 2009 Accurate bulk properties from approximate many-body techniques *Phys. Rev. Lett.* **103** 056401
[64] Caciuc V, Hölscher H and Blügel S 2005 *Ab initio* investigation of noncontact atomic force microscopy tip–surface instability in inas(110) surface *Phys. Rev.* B **72** 035423
[65] Vedmedenko E Y, Zhu Q, Kaiser U, Schwarz A and Wiesendanger R 2012 Atomic-scale magnetic dissipation from spin-dependent adhesion hysteresis *Phys. Rev.* B **85** 174410